

Stochastic natural gradient descent draws posterior samples in function space

Samuel L. Smith, Daniel Duckworth, Quoc V. Le and Jascha Sohl-Dickstein
Google Brain
{slsmith, duckworthd, qvl, jaschasd}@google.com

Abstract

Natural gradient descent (NGD) minimises the cost function on a Riemannian manifold whose metric is defined by the Fisher information. In this work, we prove that if the model predictions on the training set approach the true conditional distribution of labels given inputs, then the noise inherent in minibatch gradients causes the stationary distribution of NGD to approach a Bayesian posterior, whose temperature $T \approx \epsilon N / (2B)$ is controlled by the learning rate ϵ , training set size N and batch size B . The parameter-dependence of the Fisher metric introduces an implicit prior over the parameters, which we identify as the well-known Jeffreys prior. To support our claims, we show that the distribution of samples from NGD is close to the Laplace approximation to the posterior when $T = 1$. Furthermore, the test loss of ensembles drawn using NGD falls rapidly as we increase the batch size until $B \approx \epsilon N / 2$, while above this point the test loss is constant or rises slowly.

1 Introduction

Stochastic gradient descent remains the dominant optimization algorithm for supervised learning, but it performs poorly when the loss landscape is ill-conditioned. Natural gradient descent (NGD) provides a robust alternative based on the functional view of learning (Amari, 1998). This view observes that the model parameters ω are not important, only the function f_ω they represent. This function relates randomly sampled inputs X to a distribution over labels $Y \sim f_\omega(X)$, and the goal of learning is to uncover the true conditional distribution $P(Y|X)$. We will use $\{x, y\}$ to refer to the training set, composed of individual training examples $\{x_i, y_i\}$. A single NGD update has the form,

$$\Delta\omega = \epsilon F_x(\omega)^{-1} \left(\frac{1}{N} \frac{dC}{d\omega} \right), \quad (1)$$

where $C_{x,y}(\omega)$ is the summed cost function, N is the training set size, and $\Delta\omega = (\omega_{t+1} - \omega_t)$ is the parameter update. We pre-condition the gradient by the inverse Fisher information, $F_x(\omega)^{-1}$ (defined in Section 4), which we estimate over the training inputs (Ly et al., 2017). As the learning rate $\epsilon \rightarrow 0$, the change in function $(f_{\omega_{t+1}}(X) - f_{\omega_t}(X))$ during an update becomes independent of the model parameterization (Martens, 2014). NGD also ensures stability, by bounding the KL-divergence between functions before and after an update, such that $D_{KL}(f_{\omega_t}(X) \parallel f_{\omega_{t+1}}(X)) \leq \epsilon^2$, subject to weak requirements on the smoothness and support of $f_\omega(X)$ (Ollivier et al., 2011).

The formal properties above assume full-batch gradients, while in practice we usually estimate the gradient over small minibatches (Bottou, 2010; Robbins & Monro, 1951). Therefore in this work we analyse the influence of stochastic gradients on the stationary distribution of NGD. Our main contribution is to prove that, as the model predictions on the training set $f_\omega(x_i)$ approach the true conditional distribution $P(Y|x_i)$, this stationary distribution approaches a Bayesian posterior whose temperature $T \approx \frac{\epsilon N}{2B}$ is controlled by the ratio between the learning rate ϵ and the batch size B .

Additionally, we show NGD introduces an implicit prior over the parameters, which we identify as the well known Jeffreys prior (Jeffreys, 1946). Consistent with the functional philosophy of natural gradients, this popular default prior is both uninformative and invariant to the model parameterization (Firth, 1993; Gelman, 2009). Finally, we provide a range of experiments to support our claims:

- We show that when the batch size $B \approx \epsilon N/2$ and $N \rightarrow \infty$, the distribution of samples from NGD is close to the Laplace approximation to the true Bayesian posterior at $T = 1$.
- If the prior over parameters is chosen appropriately, then Bayesians recommend drawing inferences using ensembles sampled at $T = 1$. We observe empirically that the test loss of ensembles drawn using NGD exhibit minima close to $B \approx \epsilon N/2$. This suggests we can analytically estimate the optimal ratio between the learning rate and the batch size.

Our work builds on a number of recent works in the Bayesian community, which we discuss in Section 2. In Section 3 we derive the update rules for Langevin posterior sampling on arbitrary Riemannian manifolds, and we demonstrate how the parameter-dependence of the metric introduces a multiplicative bias to the sampling distribution. In Section 4 we consider drawing posterior samples with NGD and Gaussian noise, noting that the multiplicative bias can be interpreted as a data-dependent Jeffreys prior over the parameters. In Section 5 we combine NGD and stochastic gradients, and observe that minibatch noise drives NGD towards a stationary distribution close to a Bayesian posterior at temperature $T \approx \epsilon N/(2B)$. We present our experimental results in Section 6.

2 Related work

Langevin dynamics (Gardiner, 1985) can be used to draw posterior samples but often mixes slowly. Girolami & Calderhead (2011) proposed Riemannian Langevin dynamics, which combines Langevin dynamics and NGD to enable faster mixing when the loss landscape is poorly conditioned. However their method still requires exact gradients and remains prohibitively expensive for large training sets. Welling & Teh (2011) proposed SGLD, the first algorithm to draw posterior samples with stochastic gradients. Patterson & Teh (2013) combined SGLD with Riemannian Langevin dynamics while Li et al. (2016) combined SGLD with RMSprop. These methods scale well to large datasets but they still mix slowly, since the learning rate must satisfy the Robbins-Munro conditions (Robbins & Munro, 1951). Ahn et al. (2012) observed that the noise inherent in stochastic gradients converges to the empirical Fisher near local minima. By explicitly accounting for this noise, they draw samples from a Gaussian approximation to the posterior with finite learning rates, while converging to the exact posterior as $\epsilon \rightarrow 0$. A similar analysis was published by Mandt et al. (2017), who set the gradient preconditioner equal to the inverse of the empirical gradient covariances. These methods enable fast mixing with stochastic gradients, but the analysis in both papers only holds near local minima.

The link between natural gradients and the Jeffreys prior is mentioned in earlier work by Amari (1998), while Mahony & Williamson (2001) analysed the relationship between Riemannian manifolds and implicit priors in online learning. While we focus on exact NGD in this work, we anticipate that our conclusions could be scaled to larger networks using approximate natural gradient methods like KFAC (Martens & Grosse, 2015) or other quasi-diagonal approximations to the Fisher (Marceau-Caron & Ollivier, 2017). Zhang et al. (2017) recently proposed applying KFAC to perform variational inference, while Nado et al. (2018) combined KFAC with SGLD for posterior sampling.

3 Posterior sampling on Riemannian manifolds

The Langevin equation updates the parameters in continuous time t according to (Gardiner, 1985),

$$\frac{d\omega}{dt} = -\frac{dC}{d\omega} + \eta(t), \quad (2)$$

where $C_{x,y}(\omega)$ is the summed cost function and $\eta(t)$ denotes isotropic Gaussian noise. This noise has mean $\mathbb{E}[\eta(t)] = 0$ and covariance $\mathbb{E}[\eta(t)\eta(t')^\top] = 2TI\delta(t-t')$, where $\delta(t-t')$ is a Dirac delta function, I is the identity matrix, and T is a scalar known as the “temperature”. In the infinite time limit, Equation 2 will sample parameters from $P_{t \rightarrow \infty}(\omega) \propto e^{-C_{x,y}(\omega)/T}$. To draw samples numerically we introduce the learning rate ϵ , and integrate over a finite step of length ϵ/N to obtain,

$$\Delta\omega = -\epsilon \left(\frac{1}{N} \frac{dC}{d\omega} + \alpha \right), \quad (3)$$

where α is a Gaussian random variable with mean $\mathbb{E}[\alpha] = 0$ and covariance $\mathbb{E}[\alpha\alpha^\top] = 2TI/(\epsilon N)$. If we perform r parameter updates using Equation 3 and $\epsilon \rightarrow 0$, then we will draw a single sample from the distribution above as $t = r\epsilon/N \rightarrow \infty$. Meanwhile if the posterior is proportional to the exponentiated negative cost function, $P(\omega|x, y) \propto e^{-C_{x,y}(\omega)}$, then we sample parameters from this posterior when $T = 1$. We now generalise the Langevin equation to arbitrary Riemannian manifolds,

$$\Delta\omega = -\epsilon G_{x,y}(\omega)^{-1} \left(\frac{1}{N} \frac{dC}{d\omega} + \alpha \right). \quad (4)$$

We have introduced a symmetric, positive definite metric $G_{x,y}(\omega)$ which may depend on the training inputs, training labels and the current parameter values. In the appendix we prove Theorem 1,

Theorem 1. *We assume both $C_{x,y}(\omega)$ and $G_{x,y}(\omega)$ are Lipschitz continuous everywhere. If $\mathbb{E}[\alpha] = 0$ and $\mathbb{E}[\alpha\alpha^\top] = 2TG_{x,y}(\omega)/(\epsilon N)$, then when $\epsilon \rightarrow 0$, repeated application of Equation 4 will sample parameters from the stationary distribution $P_{t \rightarrow \infty}(\omega) \propto e^{-C_{x,y}(\omega)/T} |\det G_{x,y}(\omega)|^{1/2}$.*

This theorem differs from the analysis of Girolami & Calderhead (2011), who modified Equation 4 to account for the parameter-dependence of the metric. Theorem 1 implies one can draw posterior samples with adaptive optimizers by introducing Gaussian noise to the gradient, whose covariance is inversely proportional to the gradient pre-conditioner. However the pre-conditioner also introduces a multiplicative bias $|\det G_{x,y}(\omega)|^{1/2}$ to the sampling distribution. Notice that this bias vanishes near local minima where the pre-conditioner is constant (Ahn et al., 2012; Mandt et al., 2017).

Bayesians infer the unknown labels y_t of test inputs x_t by integrating over the posterior,

$$P(y_t|x_t, x, y) = \int d\omega P(y_t|x_t, \omega) P(\omega|x, y). \quad (5)$$

Since we cannot compute this integral exactly, in practice we draw approximate inferences by averaging our predictions over an ensemble of independent samples,

$$P(y_t|x_t, x, y) \approx \frac{1}{M} \sum_{i=1}^M P(y_t|x_t, \omega_i), \quad (6)$$

where $\omega_i \sim P(\omega_i|x, y)$, and our predictions become increasingly accurate as $M \rightarrow \infty$. Consequently if $P(\omega|x, y) \propto e^{-C_{x,y}(\omega)}$, then we expect ensembles drawn from the dynamics described in Theorem 1 to draw inferences consistent with both our prior beliefs and the training data when $T = 1$. However this may break down if the stationary distribution $P_{t \rightarrow \infty}(\omega)$ is heavily influenced by the implicit bias $|\det G_{x,y}(\omega)|^{1/2}$, which we discuss further in the following section.

4 Preconditioned Langevin dynamics and the Jeffreys prior

In this section, we apply Theorem 1 to draw posterior samples with NGD and full batch gradient estimates. For simplicity, we assume the cost function $C_{x,y}(\omega) = \sum_i \mathcal{L}(\omega, x_i, y_i) + \lambda R_x(\omega)$, where $R_x(\omega)$ is a regularizer and $\mathcal{L}(\omega, x_i, y_i) = -\ln P(y_i|x_i, \omega)$ is the cross-entropy of a unique categorical label. NGD sets the Riemannian metric $G_{x,y}(\omega)$ equal to the Fisher information,

$$F_x(\omega) = \frac{1}{N} \sum_{i=1}^N \mathbb{E}_{Y \sim f_\omega(x_i)} \left[\frac{d\mathcal{L}(\omega, x_i, Y)}{d\omega} \frac{d\mathcal{L}(\omega, x_i, Y)}{d\omega^\top} \right]. \quad (7)$$

Notice that the expectation is taken over the predicted label distribution given the current parameter values, $f_\omega(x_i)$, not the empirical labels y_i . We stated the full-batch NGD update step in Equation 1, and discussed some of its properties. To draw posterior samples we modify this update rule, introducing Gaussian noise α which satisfies $\mathbb{E}[\alpha] = 0$ and $\mathbb{E}[\alpha\alpha^\top] = 2TF_x(\omega)/(\epsilon N)$,

$$\Delta\omega = -\epsilon F_x(\omega)^{-1} \left(\frac{1}{N} \frac{dC}{d\omega} + \alpha \right). \quad (8)$$

Following Theorem 1, repeated application of Equation 8 will draw samples from $P_{t \rightarrow \infty}(\omega) \propto e^{-C_{x,y}(\omega)/T} |F_x(\omega)|^{1/2}$. The data likelihood $P(y|x, \omega) = e^{-\sum_i \mathcal{L}(\omega, x_i, y_i)}$. We introduce the temperature adjusted posterior $P_T(\omega|x, y) \propto P(y|x, \omega)^{1/T} P_T(\omega|x)$, and recall that we obtain the true

posterior $P(\omega|x, y) = P_1(\omega|x, y)$ when $T = 1$. Notice that the temperature adjusted prior $P_T(\omega|x)$ may depend on the training inputs x but not the labels y . We set $P_{t \rightarrow \infty}(\omega) = P_T(\omega|x, y)$ to identify,

$$P_T(\omega|x) \propto e^{-\lambda R_x(\omega)/T} |F_x(\omega)|^{1/2}. \quad (9)$$

The multiplicative bias introduced by the Fisher metric modifies the prior imposed by the regulariser. When $\lambda \rightarrow 0$, we obtain a temperature independent prior $P(\omega|x) \propto |F_x(\omega)|^{1/2}$, which we identify as the Jeffreys prior; a common default prior which is both uninformative and invariant to the model parameterization (Jeffreys, 1946; Firth, 1993). Like the uniform prior, the Jeffreys prior is improper. It may therefore be necessary to include additional regularisation to ensure that the posterior is well-defined. Notice that the contribution to the prior from the regulariser grows weaker as the temperature increases, matching the temperature dependence of the likelihood term. Consequently the contribution to the prior from the metric becomes increasingly dominant as the temperature rises.

Note that we can only reinterpret the multiplicative bias as a prior if the gradient pre-conditioner is independent of the training labels. However practitioners often replace the Fisher information by the empirical Fisher information, estimating the inner expectation above over the training set labels y ,

$$F_{x,y}(\omega) = \frac{1}{N} \sum_{i=1}^N \left(\frac{d\mathcal{L}(\omega, x_i, y_i)}{d\omega} \frac{d\mathcal{L}(\omega, x_i, y_i)}{d\omega^\top} \right). \quad (10)$$

5 Stochastic natural gradients and minibatch noise

We showed above how to draw posterior samples with full batch NGD and Gaussian noise. However in practice we usually estimate the gradient over a minibatch. A single stochastic NGD update has the form,

$$\Delta\omega = -\epsilon F_x(\omega)^{-1} \left(\frac{1}{N} \frac{dC}{d\omega} + \beta \right), \quad (11)$$

where the gradient noise,

$$\beta = \frac{1}{B} \left(\sum_{i=1}^B \frac{d\mathcal{L}(\omega, x_i, y_i)}{d\omega} \right) - \frac{1}{N} \left(\sum_{i=1}^N \frac{d\mathcal{L}(\omega, x_i, y_i)}{d\omega} \right). \quad (12)$$

We assume the training set is randomly sorted between each update, such that Equation 12 samples a minibatch of B training examples without replacement. Below we prove Theorem 2,

Theorem 2. *We assume both $C_{x,y}(\omega)$ and $F_x(\omega)$ are Lipschitz continuous everywhere, and that the fisher information matrix $F_x(\omega)$ is positive definite. Training inputs are drawn from a fixed distribution $P(X)$, while labels are assigned by a conditional distribution $P(Y|X)$. If $\epsilon \rightarrow 0$, $1 \ll B \ll N$, and $f_\omega(x_i) \rightarrow P(Y|x_i)$ for all observed $x_i \in x$, repeated application of Equation 11 will draw samples from $P_{t \rightarrow \infty}(\omega) \propto e^{-C_{x,y}(\omega)/T} |\det F_x(\omega)|^{1/2}$, where $T = \frac{\epsilon}{2} (\frac{N}{B} - 1)$.*

Proof. Since the gradients of individual training examples are independent,

$$\mathbb{E} \left[\frac{d\mathcal{L}(\omega, x_i, y_i)}{d\omega} \frac{d\mathcal{L}(\omega, x_j, y_j)}{d\omega^\top} \right] = \frac{1}{N^2} \left(\sum_{k=1}^N \frac{d\mathcal{L}(\omega, x_k, y_k)}{d\omega} \right) \left(\sum_{k=1}^N \frac{d\mathcal{L}(\omega, x_k, y_k)}{d\omega^\top} \right) + \Sigma_{x,y}(\omega) \delta_{ij}. \quad (13)$$

$\Sigma_{x,y}(\omega)$ denotes the empirical gradient covariances. Applying the central limit theorem over examples in the minibatch, we conclude the gradient noise β is a Gaussian random variable. By direct substitution $\mathbb{E}[\beta] = 0$, while the covariance $\mathbb{E}[\beta\beta^\top] = (\frac{N}{B} - 1)\Sigma_{x,y}(\omega)$. To compute $\Sigma_{x,y}(\omega)$, we sum Equation 13 over the indices (i, j) ,

$$\Sigma_{x,y}(\omega) = F_{x,y}(\omega) - \frac{1}{N^2} \left(\sum_{k=1}^N \frac{d\mathcal{L}(\omega, x_k, y_k)}{d\omega} \right) \left(\sum_{k=1}^N \frac{d\mathcal{L}(\omega, x_k, y_k)}{d\omega^\top} \right). \quad (14)$$

As $N \rightarrow \infty$, $\Sigma_{x,y}(\omega) \rightarrow \Sigma(\omega)$, the covariance of the underlying data distribution. Meanwhile under mild regularity conditions, $\mathbb{E}_{Y \sim f_\omega(x_i)} \left[\frac{d\mathcal{L}(\omega, x_i, Y)}{d\omega} \right] = 0$, and consequently if $f_\omega(x_i) \rightarrow P(Y|x_i)$ for all $x_i \in x$, we also obtain $F_x(\omega) \rightarrow \Sigma(\omega)$. Since we assumed $F_x(\omega) \succ 0$ this implies $\Sigma(\omega) \succ 0$, which ensures the gradient noise cannot vanish and prevents the stationary distribution from collapsing to a fixed point. Comparing equations 4 and 11 and following Theorem 1, we obtain Theorem 2. ■

This remarkable result shows that as the predictions of the model on the training set grow closer to the true conditional distribution of labels given inputs, the stationary distribution of stochastic NGD approaches a Bayesian posterior at temperature $T = \frac{\epsilon}{2} \left(\frac{N}{B} - 1 \right) \approx \epsilon N / (2B)$. As we observed in the previous section, the Fisher metric introduces a Jeffreys prior over the parameters. Our analysis builds on earlier work by Ahn et al. (2012), however their treatment assumed that the gradient preconditioner is independent of the parameters and that the posterior is described by a Gaussian distribution, while we require only that the model predictions on the training set are close to the true conditional.

Mandt et al. (2017) proposed to draw posterior samples near local minima by setting the preconditioner equal to the inverse of the empirical gradient covariances,

$$\Delta\omega = -\epsilon \Sigma_{x,y}^{-1}(\omega) \left(\frac{1}{N} \frac{dC}{d\omega} + \beta \right), \quad (15)$$

We showed above that $\mathbb{E}[\beta] = 0$ and $\mathbb{E}[\beta\beta^\top] = \left(\frac{N}{B} - 1 \right) \Sigma_{x,y}(\omega)$. Therefore by applying Theorem 1, we conclude that Equation 15 will draw samples from $P_{t \rightarrow \infty} \propto e^{-C_{x,y}(\omega)/T} |\Sigma_{x,y}(\omega)|^{1/2}$ where $T = \frac{\epsilon}{2} \left(\frac{N}{B} - 1 \right)$, so long as $\Sigma_{x,y}(\omega)$ is positive definite. This generalises the original proof provided by Mandt et al. (2017), which assumed that the gradient covariances $\Sigma_{x,y}(\omega)$ were independent of the parameters. The bias $|\Sigma_{x,y}(\omega)|^{1/2}$ cannot be interpreted as a prior, since it depends on the labels.

The metric must be positive definite, while the Fisher is positive semi-definite. To resolve this, it is common practice to introduce the modified metric $G_x(\omega) = F_x(\omega) + \delta I$ (Martens, 2014),

$$\Delta\omega = -\epsilon (F_x(\omega) + \delta I)^{-1} \left(\frac{1}{N} \frac{d\hat{C}}{d\omega} \right) \quad (16)$$

The ‘‘Fisher damping’’ δ imposes a trust region, ensuring the eigenvalues of the pre-conditioner $\epsilon(F_x(\omega) + \delta I)^{-1}$ are bounded by ϵ/δ . We therefore expect that we will be able to achieve stable training at larger learning rates by increasing δ , while we converge to exact NGD as $\delta \rightarrow 0$.

6 Experiments

6.1 Comparing preconditioned Langevin dynamics and stochastic NGD

We first consider a binary logistic regression task, with exclusive labels $y_i \in \{-1, 1\}$ and inputs x_i drawn from an n -dimensional unit Gaussian. Our model infers labels via $P(y_i|x_i, \omega) = 1/(1 + e^{y_i \omega^\top x_i})$. In Figure 1a, we show the distribution of samples from preconditioned Langevin dynamics, for which we set the metric $G_{x,y}(\omega)$ equal to the Fisher information $F_x(\omega)$, and we evaluate the gradient over the entire training set. To set the temperature, we explicitly add Gaussian noise α to the gradient of variance $\mathbb{E}[\alpha\alpha^\top] = 2TF_x(\omega)/(\epsilon N)$, as described in Section 4. Our training set comprises 1000 examples and we set the input dimensionality $n = 2$. We sample the training set

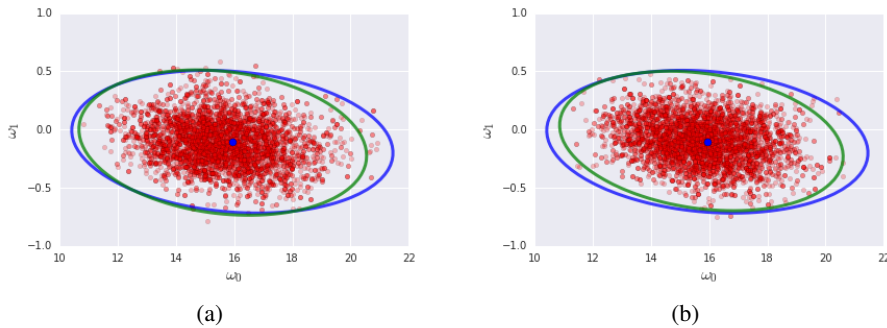


Figure 1: Samples from (a) preconditioned Langevin dynamics at $T = 1$ and (b) NGD when the batch size $B = \epsilon N / 2$. We plot the iterates in red, the Laplace approximation to the posterior in blue and the covariance of the iterates in green (to 3 standard deviations). As predicted, the stationary distributions of preconditioned Langevin dynamics and stochastic NGD are remarkably similar.

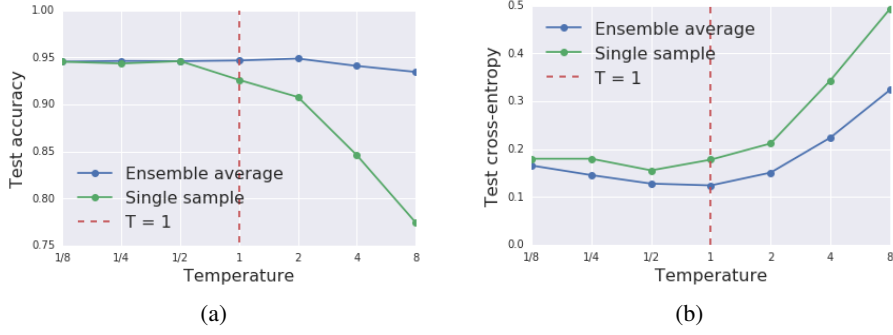


Figure 2: Preconditioned Langevin dynamics for logistic regression. The test set accuracy (a) and test cross-entropy (b), as a function of the sampling temperature T , which we set by adding Gaussian noise to the gradient. The test cross-entropy of the ensemble is minimised at $T = 1$.

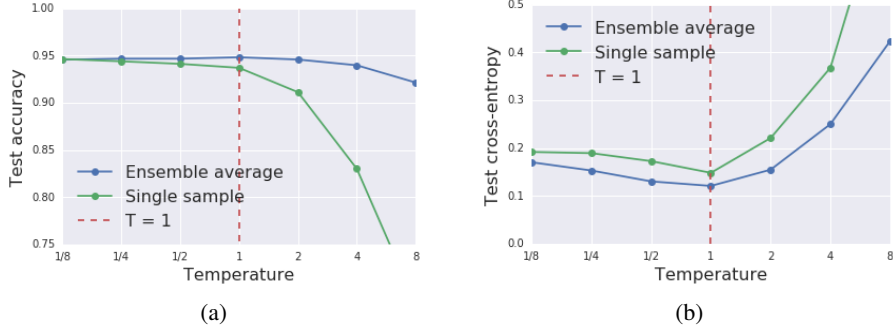


Figure 3: NGD for logistic regression. The test set accuracy (a) and test cross-entropy (b), as a function of the sampling temperature T , which we control by setting the batch size $B = \epsilon N / (2T)$. As predicted, the performance of the ensemble is similar to preconditioned Langevin dynamics.

labels of each input from the Bernoulli distribution of the “true” parameter values $\omega_{true} = (16, 0)$. The learning rate $\epsilon = 0.1$ and the Fisher damping $\delta = 10^{-4}$. We first run 5000 parameter updates to burn in, before sampling the following 5000 parameter values. The blue point denotes the cost function minimum, obtained by LBFGS, while the blue curve illustrates the width of the Bayesian posterior (to 3 standard deviations), estimated using the Laplace approximation. To confirm that the samples are drawn from a distribution close to the posterior, we plot the covariance of the samples in green. In Figure 1b we replace preconditioned Langevin dynamics by NGD. To set $T = 1$, we simply estimate the gradient over minibatches of size $B = \epsilon N / 2 = 50$. Batches are sampled randomly without replacement, and we continue to estimate the Fisher information over the full training set. As predicted, when we set the batch size correctly the stationary distribution of NGD is close to the posterior, drawing samples from the same distribution as preconditioned Langevin dynamics.

We now increase the difficulty of the task by setting the input dimensionality $n = 64$ and the true parameter values $w_{true} = (16, 0, 0, 0, \dots, 0)$, such that the input comprises one relevant feature and 63 irrelevant features. In Figure 2, we plot the mean test set accuracy and test cross entropy of preconditioned Langevin dynamics as we vary the temperature T . Once again, we set the learning rate $\epsilon = 0.1$ and the damping $\delta = 10^{-4}$, and we run 1000 parameter updates to burn in. In blue we plot the performance of a conventional ensemble average over the final 1000 parameter values, while in green we plot the accuracy of a single sample. The ensemble outperforms single parameter samples, and the test cross entropy of the ensemble is minimised when $T = 1$. Meanwhile in Figure 3, we plot the test set accuracy and test cross entropy of NGD on the same task. We continue to estimate the Fisher over the full training set, but we sample the gradient using minibatches of size $B = \epsilon N / (2T)$. As predicted by our theoretical analysis, the performance of NGD is remarkably similar to preconditioned Langevin dynamics, and the test cross entropy is minimised at $T = \epsilon N / (2B) = 1$.

6.2 Changing the implicit prior can change the optimal temperature

We expect posterior samples drawn at $T = 1$ to perform well, so long as the prior over parameters was chosen well. However choosing a sensible prior is challenging, and if we choose the prior poorly, then the optimal temperature may shift. To investigate this phenomenon, we explore the influence of the implicit prior $P(\omega) \propto |F_x(\omega) + \delta I|^{1/2}$ on the logistic regression task introduced above. The hyper-parameter δ specifies the Fisher damping, and we recover the Jeffreys prior when $\delta \rightarrow 0$. Since the training inputs are sampled from an isotropic multi-dimensional Gaussian, in the limit $N \rightarrow \infty$ we expect this prior to depend only on the L2 norm of the parameters $|\omega|$. Therefore in figure 4a, we plot the implicit prior for a range of Fisher damping values, as we move in the direction of the true parameters (the choice of direction is arbitrary since the prior does not depend on the labels). We find that in this simple model, the Jeffreys prior introduces a penalty on the parameter norm. As the Fisher damping coefficient increases, the strength of this penalty is reduced. Finally in figure 4b, we plot the test cross-entropy of NGD as a function of temperature. This plot is identical to Figure 3b, except that we increase the Fisher damping to $\delta = 10^{-2}$, which increases the optimal temperature to $T \sim 2$.

These results suggest that in this simple model, the Jeffreys prior is beneficial and aids generalization. However there is no guarantee that the Jeffreys prior will be beneficial in other model architectures. In particular, it is well known that the Fisher matrix is close to the Hessian near local minima (Martens, 2014), and consequently the Jeffreys prior will drive the parameters away from “flat” minima whose Hessian eigenvalues are small towards “sharp” minima where the Hessian determinant is large. In deep learning, it is widely thought that sharp minima generalise poorly (Hochreiter & Schmidhuber, 1997; Keskar et al., 2016), and so we speculate that implicit priors may explain the recent observation that adaptive optimisers often perform worse on the test set than SGD (Wilson et al., 2017).

6.3 Stochastic NGD and an MLP

To confirm that our conclusions are relevant to non-convex settings we now apply NGD to train a simple MLP on MNIST. Our model has a single hidden layer with 40 hidden units and RELU activations. To reduce the number of parameters, we use a matrix whose elements are drawn randomly from the unit Gaussian to project the input features down to 10 dimensions, and to emphasize the influence of the temperature on training we reduce the training set size to $N = 1024$. We also found it was necessary to include additional regularisation to ensure the samples converge to a stationary distribution. We therefore introduce L2-regularization with regularization coefficient $\lambda = 20.0/N$. We increase the Fisher damping to $\delta = 0.1$ to ensure stability, while the learning rate $\epsilon = 1/8$. In Figure 5a, we plot the test set accuracy of NGD as a function of the batch size used to estimate the gradient. The Fisher is estimated over separate batches of 1024 images, using a single sampled label per example. For each batch size, we perform 500 gradient updates to burn in, before sampling the parameters over a further 500 updates. We plot both the performance of the ensemble average across the 500 samples, as well as the mean accuracy of a single sample. When training with an ensemble, the accuracy increases rapidly as we increase the batch size until we reach $B = \epsilon N/2 = 64$, at which

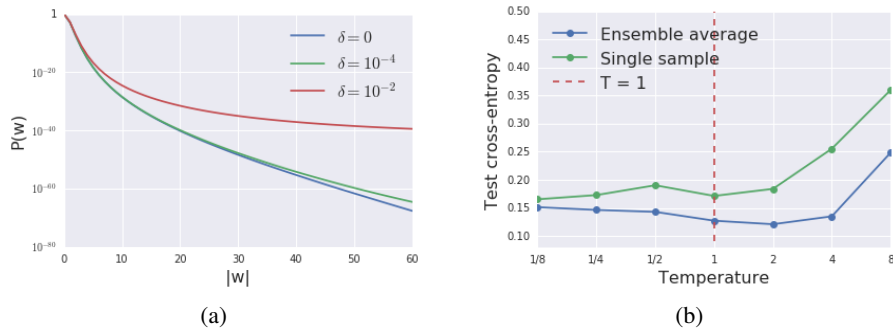


Figure 4: a) The implicit prior for logistic regression on simulated data as a function of the L2 norm of the parameters, for a range of values of the Fisher damping δ . b) The test cross-entropy of logistic regression as a function of the temperature $T = \epsilon N/(2B)$, when the Fisher damping $\delta = 10^{-2}$. Increasing the Fisher damping softens the implicit prior, and this changes the optimal temperature.

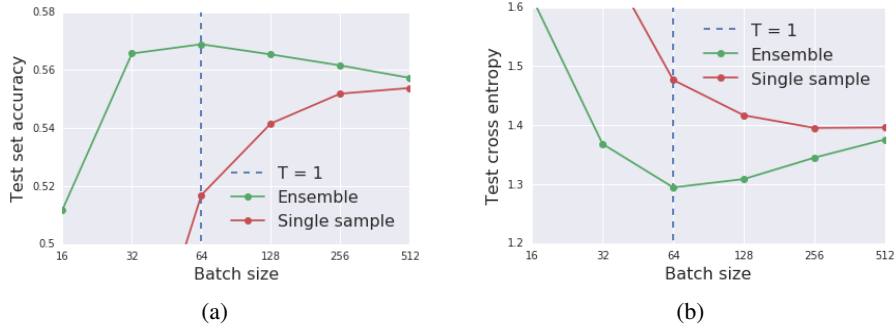


Figure 5: The test set accuracy (a) and test cross entropy (b) of NGD as a function of batch size B , when training an MLP on 10 randomly projected input features from MNIST with $N = 1024$. We also provide the batch size $B = 2N/\epsilon$ at which the temperature $T = 1$. We note that the peak test accuracy is very low, since this task is substantially harder than classifying a complete MNIST image.

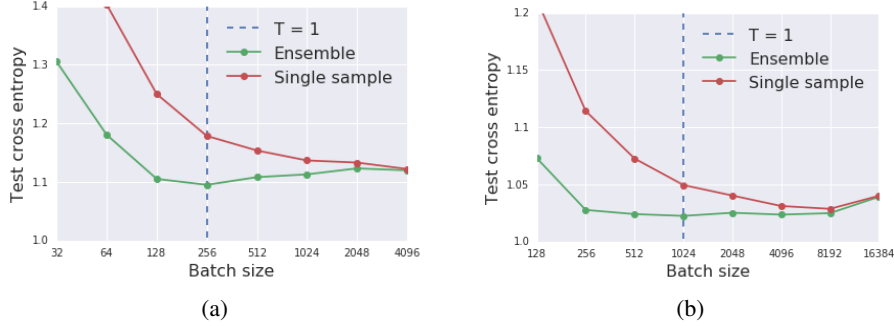


Figure 6: The test cross entropy of NGD as a function of batch size B , when training an MLP on 10 randomly projected input features from MNIST. a) The training set size $N = 4096$. The cross-entropy of the ensemble shows a minimum at $B = 256$, for which $T = \epsilon N/(2N) = 1$. b) The training set size $N = 16384$. As the training set size increases, the minimum near $T \approx 1$ is increasingly flat.

the temperature $T = 1$, while above this temperature the accuracy drops (as we showed above, this optimum may exhibit a weak dependence on the damping coefficient or the regulariser). In Figure 5b, we exhibit the test set cross-entropy. While the mean test cross-entropy of a single sample always rises as we reduce the batch size, the ensemble test cross-entropy also shows a minimum at $B = 64$.

In Figure 6a we exhibit the test cross entropy for the same model when we increase the training set size to $N = 4096$. Now the cross entropy of the ensemble shows a minimum at an increased batch size of $B = 256$. Once again, this matches the Bayesian prediction. Notice that this leads to a linear scaling rule between the batch size and the training set size ($B \propto N$) as was previously observed for SGD by Smith & Le (2018). In Figure 6b, we further increase the training set size to $N = 16384$. The minimum in the test cross entropy becomes increasingly flat as the training set grows.

6.4 Stochastic NGD and a CNN

In Figure 7, we apply NGD to train a CNN on MNIST. Our model is comprised of 3 convolutional layers and 1 fully connected softmax layer. Each convolutional layer has a $(3, 3)$ spatial window, 10 output channels and a stride of 2. This results in a total of 3490 trainable parameters (1890 for the convolutional layers and 1600 for the final fully connected layer). We introduce L2 regularization and set $\lambda = 40.0/N$. The Fisher information is estimated during training using independent minibatches of 1024 examples, using a single sampled label per example. To reduce variance, we store a moving average of the Fisher over previous updates, and we set the smoothing coefficient of the Fisher moving average, $\alpha = 0.95^{(\epsilon/0.001)}$. The Fisher damping $\delta = 0.1$. To reduce the burn in time, we initialise the weights at the start of training from the final parameters of a single SGD training run on

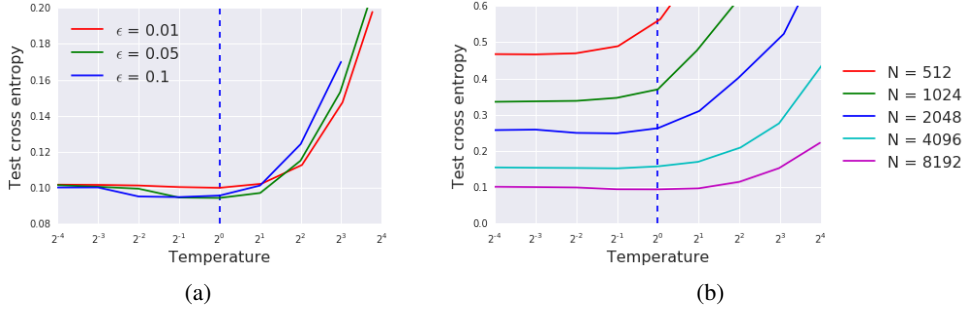


Figure 7: The test cross entropy of NGD as a function of temperature $T = \frac{\epsilon}{2} \left(\frac{N}{B} - 1 \right)$, when training a CNN on MNIST. a) The training set size $N = 8192$, and we plot the test cross entropy as a function of temperature T , for a range of learning rates ϵ . b) The learning rate $\epsilon = 0.05$, and we plot the test cross entropy as a function of temperature for a range of training set sizes N .

the full MNIST training set. We average our predictions over ensembles sampled from the final 0.2% of gradient updates at the end of training, and we perform $\lceil 850/\epsilon \rceil$ gradient updates per training run.

In Figure 7a, we plot the test cross entropy when the training set size, $N = 8192$, for a range of learning rates ϵ . We set the temperature by choosing the batch size $B = \lceil N / (\frac{2T}{\epsilon} + 1) \rceil$. As expected, the test cross entropy at constant temperature is largely independent of the learning rate, indicating that stochastic NGD obeys a linear scaling rule between batch size and learning rate, $B \propto \epsilon$ when $B \ll N$, as already observed by many authors for SGD (Goyal et al., 2017; Smith et al., 2018; Balles et al., 2016). The test cross entropy for all learning rates rises rapidly once $T > 1$. In Figure 7b, we exhibit the test cross entropy when $\epsilon = 0.05$ for a range of training set sizes. The test cross entropy rises as the size of the training set falls, but we consistently observe that the test cross entropy begins to increase rapidly once $T \gtrsim 1$. The minimum exhibits a weak shift towards smaller temperatures for smaller training sets. Since the implicit prior becomes increasingly dominant as the training set shrinks, this may indicate that the Jeffreys prior is detrimental to learning in this architecture.

7 Conclusions

We prove that, as the model predictions on the training set approach the true conditional distribution between inputs and labels, the stationary distribution of natural gradient descent approaches a Bayesian posterior at a temperature $T \approx \epsilon N / (2B)$ controlled by the learning rate ϵ , training set size N , and the batch size B . This posterior is modified by a multiplicative bias, which can be interpreted as an implicit Jeffreys prior over the parameters. To confirm our claims, we demonstrate that samples from NGD at $B = \epsilon N / 2$ are close to the Laplace approximation to the Bayesian posterior. We also find that the test cross entropy of ensembles sampled from NGD are minimised when $B \approx \epsilon N / 2$. These results confirm minibatch noise can improve the generalization performance of NGD, and suggest Bayesian principles may help us predict the optimal batch size to use during training.

Acknowledgements

We thank Martin Abadi for helpful discussions and Matthew Johnson, Matt Hoffman, Roger Grosse and Yasaman Bahri for feedback on an earlier draft of this paper.

References

- Sungjin Ahn, Anoop Korattikara, and Max Welling. Bayesian posterior sampling via stochastic gradient fisher scoring. *arXiv preprint arXiv:1206.6380*, 2012.
- Shun-Ichi Amari. Natural gradient works efficiently in learning. *Neural computation*, 10(2), 1998.
- Lukas Balles, Javier Romero, and Philipp Hennig. Coupling adaptive batch sizes with learning rates. *arXiv preprint arXiv:1612.05086*, 2016.

- Léon Bottou. Large-scale machine learning with stochastic gradient descent. In *Proceedings of COMPSTAT'2010*, pp. 177–186. Springer, 2010.
- David Firth. Bias reduction of maximum likelihood estimates. *Biometrika*, 80(1):27–38, 1993.
- Crispin W Gardiner. *Handbook of Stochastic Methods*, volume 4. Springer Berlin, 1985.
- Andrew Gelman. Bayes, jeffreys, prior distributions and the philosophy of statistics. *Statistical Science*, 24(2):176–178, 2009.
- Mark Girolami and Ben Calderhead. Riemann manifold langevin and hamiltonian monte carlo methods. *Journal of the Royal Statistical Society: Series B*, 73(2):123–214, 2011.
- Priya Goyal, Piotr Dollár, Ross Girshick, Pieter Noordhuis, Lukasz Wesolowski, Aapo Kyrola, Andrew Tulloch, Yangqing Jia, and Kaiming He. Accurate, large minibatch SGD: Training imagenet in 1 hour. *arXiv preprint arXiv:1706.02677*, 2017.
- Sepp Hochreiter and Jürgen Schmidhuber. Flat minima. *Neural Computation*, 9(1):1–42, 1997.
- Harold Jeffreys. An invariant form for the prior probability in estimation problems. *Proceedings of the Royal Society of London. Series A, Mathematical and Physical Sciences*, pp. 453–461, 1946.
- Nitish Shirish Keskar, Dheevatsa Mudigere, Jorge Nocedal, Mikhail Smelyanskiy, and Ping Tak Peter Tang. On large-batch training for deep learning: Generalization gap and sharp minima. *arXiv preprint arXiv:1609.04836*, 2016.
- Chunyu Li, Changyou Chen, David E Carlson, and Lawrence Carin. Preconditioned stochastic gradient langevin dynamics for deep neural networks. In *AAAI*, volume 2, pp. 4, 2016.
- Alexander Ly, Maarten Marsman, Josine Verhagen, Raoul PPP Grasman, and Eric-Jan Wagenmakers. A tutorial on fisher information. *Journal of Mathematical Psychology*, 80:40–55, 2017.
- Robert E Mahony and Robert C Williamson. Prior knowledge and preferential structures in gradient descent learning algorithms. *Journal of Machine Learning Research*, 1(Sep):311–355, 2001.
- Stephan Mandt, Matthew D Hoffman, and David M Blei. Stochastic gradient descent as approximate bayesian inference. *arXiv preprint arXiv:1704.04289*, 2017.
- Gaétan Marceau-Caron and Yann Ollivier. Natural langevin dynamics for neural networks. In *International Conference on Geometric Science of Information*, pp. 451–459. Springer, 2017.
- James Martens. New insights and perspectives on the natural gradient method. *arXiv preprint arXiv:1412.1193*, 2014.
- James Martens and Roger Grosse. Optimizing neural networks with kronecker-factored approximate curvature. In *International conference on machine learning*, pp. 2408–2417, 2015.
- Zachary Nado, Jasper Snoek, Roger Grosse, David Duvenaud, Bowen Xu, and James Martens. Stochastic gradient langevin dynamics that exploit neural network structure. *International Conference on Learning Representations 2018 (Workshop)*, 2018.
- Yann Ollivier, Ludovic Arnold, Anne Auger, and Nikolaus Hansen. Information-geometric optimization algorithms: A unifying picture via invariance principles. *arXiv:1106.3708*, 2011.
- Sam Patterson and Yee Whye Teh. Stochastic gradient riemannian langevin dynamics on the probability simplex. In *Advances in Neural Information Processing Systems*, pp. 3102–3110, 2013.
- Herbert Robbins and Sutton Monro. A stochastic approximation method. *The annals of mathematical statistics*, pp. 400–407, 1951.
- Samuel L. Smith and Quoc V. Le. A bayesian perspective on generalization and stochastic gradient descent. *ICLR*, 2018.
- Samuel L. Smith, Pieter-Jan Kindermans, and Quoc V. Le. Don’t decay the learning rate, increase the batch size. *ICLR*, 2018.

Max Welling and Yee W Teh. Bayesian learning via stochastic gradient langevin dynamics. In *Proceedings of the 28th International Conference on Machine Learning*, pp. 681–688, 2011.

Ashia C Wilson, Rebecca Roelofs, Mitchell Stern, Nathan Srebro, and Benjamin Recht. The marginal value of adaptive gradient methods in machine learning. *arXiv preprint arXiv:1705.08292*, 2017.

Guodong Zhang, Shengyang Sun, David Duvenaud, and Roger Grosse. Noisy natural gradient as variational inference. *arXiv preprint arXiv:1712.02390*, 2017.

Appendix

To prove Theorem 1, we apply a basis transformation to the conventional Langevin equation, into a new set of parameters ω' . We introduce a Riemannian distance metric $G(\omega')$, which is both symmetric and positive definite, such that $G(\omega') = B(\omega')B^\top(\omega')$ (Girolami & Calderhead, 2011). The transformation between the two bases is defined by the measure,

$$|d\omega|^2 = d\omega^\top d\omega = d\omega'^\top G(\omega') d\omega' \quad (17)$$

$$= d\omega'^\top B(\omega')B(\omega')^\top d\omega' \quad (18)$$

$$= |B(\omega')^\top d\omega'|^2, \quad (19)$$

from which we identify $d\omega = B(\omega')^\top d\omega'$. Applying this basis transformation to Equation 2 from Section 3 of the main text,

$$B(\omega')^\top \frac{d\omega'}{dt} = -B(\omega')^{-1} \frac{dC}{d\omega'} + \eta(t), \quad (20)$$

and thus¹,

$$\frac{d\omega'}{dt} = -G(\omega')^{-1} \frac{dC}{d\omega'} + \eta'(t), \quad (21)$$

where we have defined $\eta'(t)$ such that $\mathbb{E}[\eta'(t)\eta'(t')^\top] = 2TB(\omega')^\top B(\omega')^{-1} = 2TG(\omega')^{-1}$. Equation 2 generates samples from $P_{t \rightarrow \infty}(\omega) \propto e^{-C(\omega)/T}$, and the basis transformation must obey,

$$|P_{t \rightarrow \infty}(\omega') d\omega'| = |P_{t \rightarrow \infty}(\omega) d\omega|. \quad (22)$$

Therefore,

$$P_{t \rightarrow \infty}(\omega') = P_{t \rightarrow \infty}(\omega) \left| \det \left(\frac{d\omega}{d\omega'} \right) \right| \quad (23)$$

$$\propto e^{-C(\omega)/T} |\det B(\omega')^\top| \quad (24)$$

$$= e^{-C(\omega')/T} |\det G(\omega')|^{1/2}. \quad (25)$$

We define $C(\omega') = C(\omega)$ everywhere. We now integrate Equation 21 over a finite step,

$$\Delta\omega' = \int_0^{\epsilon/N} \frac{d\omega'}{dt} dt \quad (26)$$

$$= \epsilon G(\omega')^{-1} \left(\frac{1}{N} \frac{dC}{d\omega'} \right) + \alpha. \quad (27)$$

The Gaussian random variable α has mean $\mathbb{E}[\alpha] = \int_0^{\epsilon/N} \mathbb{E}[\eta'(t)] dt = 0$, and covariance $\mathbb{E}[\alpha\alpha^\top] = \int_0^{\epsilon/N} \int_0^{\epsilon/N} \mathbb{E}[\eta'(t)\eta'(t')^\top] dt dt' = 2\epsilon TG(\omega')^{-1}/N$. As $\epsilon \rightarrow 0$, repeatedly applying Equation 27 will converge to the stationary distribution of Equation 25. From now on we will forget the original parameter basis and let $\omega' \rightarrow \omega$. For later convenience, we can re-express the update rule,

$$\Delta\omega = \epsilon G(\omega)^{-1} \left(\frac{1}{N} \frac{dC}{d\omega} + \alpha \right), \quad (28)$$

where now $\mathbb{E}[\alpha] = 0$, and $\mathbb{E}[\alpha\alpha^\top] = 2TG(\omega)/(\epsilon N)$. Thus completing our proof.

¹Notice that $\frac{d}{d\omega} = B(\omega')^{-1} \frac{d}{d\omega'}$, not $B(\omega')^\top B(\omega')^{-1} \frac{d}{d\omega'}$.